Separation Science and Technology
Publication details, including instructions for authors and subscription information:
http://www.informaworld.com/smpp/title~content=t713708471

Computational Fluid Dynamics Simulation of High Gradient Magnetic Separation

Hidehiko Okada[a]; Kazunari Mitsuhashi[b]; Takeshi Ohara[c]; Evan R. Whitby[d]; Hiroshi Wada[b]
[a] National Institute for Materials Science, Tsukuna, Japan [b] University of Tokyo, Kashiwa, Japan [c] Kanazawa Institute of Technology, Kanazawa, Japan [d] Chimera Technologies, Inc, Minnesota, USA

To cite this Article Okada, Hidehiko , Mitsuhashi, Kazunari , Ohara, Takeshi , Whitby, Evan R. and Wada, Hiroshi(2005) 'Computational Fluid Dynamics Simulation of High Gradient Magnetic Separation', Separation Science and Technology, 40: 7, 1567 — 1584
To link to this Article: DOI: 10.1081/SS-200056063
URL: http://dx.doi.org/10.1081/SS-200056063

Separation Science and Technology, 40: 1567–1584, 2005

ISSN 0149-6395 print/1520-5754 online
DOI: 10.1081/SS-200056063

Computational Fluid Dynamics Simulation of High Gradient Magnetic Separation

Hidehiko Okada
National Institute for Materials Science, Tsukuna, Japan

Kazunari Mitsuhashi
University of Tokyo, Kashiwa, Japan

Takeshi Ohara
Kanazawa Institute of Technology, Kanazawa, Japan

Evan R. Whitby
Chimera Technologies, Inc, Minnesota, USA

Hiroshi Wada
University of Tokyo, Kashiwa, Japan

Abstract: A computational fluid dynamics (CFD) model was developed for High Gradient Magnetic Separation (HGMS) of particles in liquids flowing through magnetic filters. Using this model, we simulated the effect of fluid flow, magnetic forces, and particle diffusion on the particle filtration efficiency in an HGMS liquid particle filter. By simulating capture efficiency of the simple configuration, the overall filtration efficiency of HGMS filters can be determined. This paper describes this numerical model and simulation results for an HGMS liquid particle filter.

Keywords: Computer simulation, computational fluid dynamics, high gradient magnetic separation, suspended fine particles

Received July 6, 2004, Accepted February 6, 2005
Address correspondence to Hidehiko Okada, National Institute for Materials Science, Tsukuna Magnet Laboratory, 3-13 Sakura, Tsukuna, Ibaraki 305-0003, Japan. Tel.: 81-29-851-3354 extn. 5039; Fax: 81-29-851-5441; E-mail: okada.hidehiko@nims.go.jp

INTRODUCTION

High Gradient Magnetic Separation (HGMS) was developed almost 30 yrs ago (1–3), and is a powerful technique for separating substances dispersed in liquids. HGMS has been used to purify Kaolin clay in the paper-coating industry (4), to purify wastewater in the steel industry (5), and to remove iron compounds from boiler feed water in thermal and nuclear power plants (6, 7). Because of the development of economical and reliable cryocooler-cooled superconducting magnets, HGMS systems can now be easily applied to other separation processes as well (8). Combining new superconducting technology with existing HGMS systems improves the performance of existing HGMS systems and permits the development of new filtration systems with filtration efficiency and ease of cleaning not possible with existing filtration systems. HGMS systems capture magnetized particles on the surface of a matrix of magnetized wires as follows. An external magnetic field is applied to a matrix of magnetic wires, thus creating magnetic field gradients that attract particles to the matrix. Because magnetic wire matrices release caught particles if the external magnetic field is turned off, magnetic filters can be easily cleaned and reused. Compared with traditional filtration systems, this is a feature unique to HGMS systems. Meanwhile, a wire for HGMS is a micro device to control motion of magnetized fine particles. From this point of view, HGMS is one of promising methods to sort nano-particles (10, 11) or control motion of magnetic beads for biomedicine (12).

Despite many past works (13–37), the effect of operating conditions of such HGMS systems on the particle filtration efficiency is still not sufficiently well understood to properly design efficient filters that use this technology. We therefore developed a numerical model to study the effect of system operating parameters on the particle filtration efficiency. Our goal was to use this model to explain observed HGMS filtration characteristics and to use the model to develop new magnetic filtration systems.

In HGMS systems, magnetized particles are transported by convection of the suspending fluid and are drawn to magnetic wires by magnetic forces exerted on the particles. The magnetic force on the particles is a function of the magnetic field strength and magnetic field gradients near the filter wire. Viscous drag of the suspending fluid on the particles retards the motion of the particles, and particle diffusion also decreases the net flux of particles due to external forces such as magnetic forces. Particles that contact the magnetic wires are trapped on the wire. To study HGMS phenomena, therefore, the combined effect of fluid convection, magnetic fields, and particle diffusion on the motion of particles must be considered. Therefore, a combination of electro-magnetic, fluid, and particle dynamics models is required.

A Particle Trajectory Model (13–21), which solves particle trajectories by solving an equation of motion for each particle for each device, is one of

the most conventional models. Models based on the Particle Trajectory model are used in the recent works (22, 24, 25, 27–30). However, particle diffusion also influences magnetic separation of fine particles, especially for particles smaller than about 100 nm. Previous studies indicate that distributions of particle concentration are controlled by combined magnetic attraction and diffusion of particles in the neighborhood of magnetic wires, and the build-up of particles on a filament in quiescent water has been estimated (33–37). To simulate HGMS systems, a method is therefore required for simulating the combined effect of fluid convection, particle diffusion, and magnetic forces on the motion of particles.

SIMULATION OF HGMS

Model of HGMS Processes

Particle trajectory models (13–21) are often used to study HGMS processes. Particle trajectory models solve Newton's equation of motion to trace particle motion. A capture radius can be determined by using these models, which defines the region around a wire within which particles are captured. However, Newton's equation of motion does not account for diffusion. The Langeven equation of motion with a random force can describe stochastic processes such as diffusion, but because particle motion described by the Langeven equation is a random walk, a capture radius cannot be defined in the same way as with the particle trajectory model.

Another option is to use computational fluid dynamics (CFD) models to simulate HGMS processes, because CFD models solve a convection-diffusion equation that includes the effect of fluid convection and diffusion on the motion of a scalar species like particles. The general transport equation (38) used in CFD models can be described as

$$\frac{\partial}{\partial t}(\rho\phi) + \vec{\nabla}(\rho\vec{u}\phi) = \vec{\nabla}\cdot(\Gamma\vec{\nabla}\phi) + S, \tag{1}$$

where ρ is the fluid density, ϕ is the transported scalar variable, which in this study was particle mass fraction, $\vec{u}$ is the fluid velocity, Γ is the scalar diffusion constant, and S is the scalar source term. From left to right, the four terms in (1) are commonly referred to as the unsteady, convection, diffusion, and source terms.

In HGMS systems, particle motion is also affected by magnetic forces, which are referred to as an external force. We neglect the effect of gravitational forces, because for particles with diameter, $d_p < 1\,\mu m$, gravitational velocities in water are negligible for the time scales of interest in HGMS systems. To modify (1) to account for the effect of magnetic forces on particles, we must determine the force on particles due to magnetic

forces and the restraining force due to viscous drag. The magnetic force acting on a substance with magnetization, M, in a magnetic field, H, is given by

$$\vec{F} = \frac{1}{2}\vec{\nabla}(\vec{M} \cdot \vec{H}), \tag{2}$$

when

$$\vec{M} = \mu_0 \chi \vec{H}, \tag{3}$$

where μ_0 is the vacuum magnetic permeability and χ is the relative magnetic susceptibility. Namely, the magnetic force can be written as follows,

$$\vec{F} = \mu_0 \chi |\vec{H}| \vec{\nabla} |\vec{H}|. \tag{4}$$

For spherical particles, the external velocity, $\vec{u}_{\text{ext}}$, caused by the magnetic force can be calculated as follows by using Stokes' law of fluid drag on particles to account for viscous drag:

$$\vec{u}_{\text{ext}} = \frac{\vec{F}}{6\pi\eta b}, \tag{5}$$

where b is the particle radius and η is the dynamic viscosity coefficient. The particle velocity, $\vec{u}_{\text{p}}$, can therefore be calculated as

$$\vec{u}_{\text{p}} = \vec{u}_{\text{ext}} + \vec{u}. \tag{6}$$

Substituting $\vec{u}_{\text{p}}$ for $\vec{u}$ in (1) yields the general equation for calculating the particle motion due to the combined effects of fluid convection, external forces, and diffusion. In this model, therefore, the effect of the magnetic field is introduced through $\vec{u}_{\text{ext}}$.

In ref. [43], the same model succeeded in simulating a magnetic chromatograph, which is a measuring technique of ions or fine particles using HGMS (44).

Calculation Procedure

Additional assumptions in the model are that the particles are spherical, there are no particle-particle interactions, the fluid flow is two-dimensional and laminar, and the magnetic field is steady. Although we also assumed that all wires were circular, our model can also be used to simulate the effect of wires of arbitrary shape.

The magnetic field is obtained by calculating the gradient of the magnetic potential derived by Poisson's equation. Because the fluid and external velocities must be given to solve (1), the Navier-Stokes equation must be solved to

determine the distribution of the fluid velocity and the Poisson equation must be solved for the distribution of the magnetic field. Because both the Navier-Stokes and Poisson equations have the same general form as (1), CFD models can be used to solve for the fluid velocity distribution, magnetic field, and particle concentration distribution. Neglecting the left-hand side of (1), setting $\Gamma = 1$, and substituting the distribution of magnetic charge into S, Eq. (1) becomes the Poisson equation for magnetic potential. By defining ρ as fluid density, $\vec{u}$ as fluid velocity, Γ as dynamic fluid viscosity, and substituting a suitable pressure term into S, Eq. (1) becomes the Navier-Stokes equation and can be used to solve for the velocity profile. Finally, defining ρ as fluid density, Γ as particle diffusion coefficient, and substituting $\vec{u}_p$ for $\vec{u}$, Eq. (1) becomes an equation that defines the distribution of particle concentration. In the following calculations Γ is obtained by Einstein's relation for a spherical particle. The particle capture ratio and other useful characteristics of the filtration system can therefore be calculated from simulations that include the Navier-Stokes, Poisson, and particle dynamics equations.

The solution of (1) is complex, and we used a commercially available finite-volume method (FVM) CFD program, COMPACT (Innovative Research Inc.), to numerically solve (1). A description of the FVM technique is given by (38, 39).

CALCULATIONS

Calculation Model

Because our system is composed of many magnetic filter wires in a repeating pattern, we solved (1) assuming periodic boundary conditions in the y-direction. In the simulation, the external magnetic field and fluid flow were in the x-direction, and a single filter wire was oriented in the z-direction. Because we used a magnetic field strong enough to saturate the magnetization of the wire, we assumed that the saturated magnetization of the wire was 1.6 T. This value corresponds to the typical saturated magnetization of stainless steel. For all simulations we used a particle relative susceptibility of 2×10^{-3}, which is typical for paramagnetic materials, and the particle diameter is 1 μm. The initial particle mass fraction for all simulations was 0.001, and particles were dispersed in water with a relative magnetic susceptibility of -7.2×10^{-7} and the dynamic viscosity coefficient of $1.0 \times 10^{-6} \mathrm{m}^2/\mathrm{s}$.

In calculating the fluid velocity distribution, we set the inlet velocity at $X = 0$ as the boundary condition.

In the magnetic filter system, the accumulation of trapped particles deforms the surface of the filament. To simplify our simulations, however, we assumed that particles did not accumulate on the filter wire surface and therefore did not affect either the shape or magnetic properties of the wire.

Capture ratio is an important indicator of the efficiency of the magnetic filter. Usually the capture ratio of a filter is defined as

$$capture\ ratio = 1 - \frac{J_{out}}{J_{in}}, \tag{7}$$

where J_{in} is the particle mass flux at the inlet and J_{out} is the particle mass flux at the outlet.

To examine details of the filter, we show the capture ratio of each wire in a filter in the following sections. In that calculation we also define bounds around the wire. We consider flux density crossing the bounds as flux density flowing to the wire.

Concentration and Deposition on a Single Filter Wire

Figure 1 shows the distribution of magnetic potential and magnetic fields around a magnetic wire with a diameter of 500 μm in a homogeneous external field, $|\mu_0 H|$, of 5 T and fiber-fiber distance of 2.5 mm in the y-direction. We omitted external homogeneous magnetic fields in the magnetic field shown in Fig. 1, because homogeneous magnetic fields do not contribute to the magnetic force except magnetization of particles, as shown in (3) and (4).

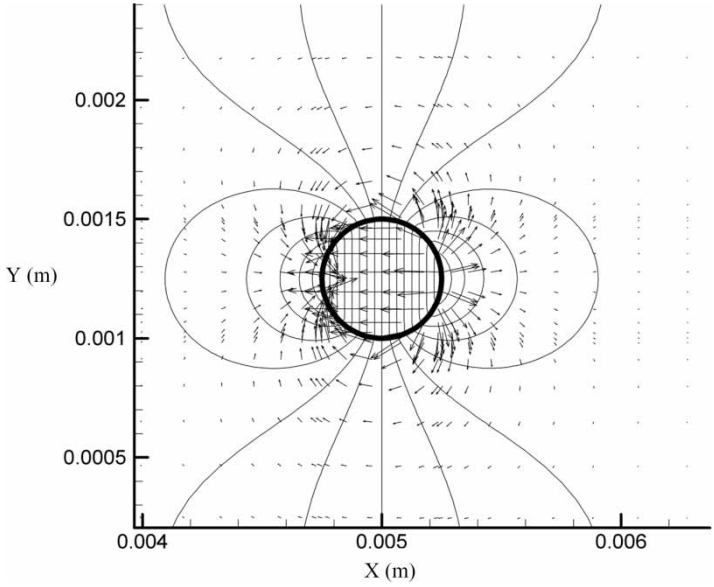

Figure 1. Magnetic field near a magnetic filter wire (thick, circular outline in the center). Vectors show magnetic field. Contour lines show magnetic potential.

We can verify that for paramagnetic particles with positive magnetic susceptibility, the magnetic forces are attractive near the upstream and downstream sides of the wire, but repulsive near the other sides.

Because we use a periodic boundary condition to simulate the effect of multiple wires, in contrast to an isolated wire, the contours of magnetic potential shown in Fig. 1 are distorted by multiple, neighboring filter wires in the y-direction (shown with a thick, circular line in the middle of Fig. 1).

Figure 2 shows the distribution of fluid velocity for an inlet velocity of 0.1 m/s and for Reynolds number, Re = 50. Note that there are two eddies behind the filter wire and that some of the velocity vectors are small (indicating low velocity) and point toward the filter wire, in the direction opposite to the main flow direction (40–42). Figures 1 and 2 show that our model gives distribution of magnetic field and flow exactly.

Figure 3 shows the particle mass fraction near a single wire with a diameter of 500 μm for an inlet mass fraction of 0.001. Figure 3 shows a cross-section cut along the X-axis at the center of the same wire. The black solid lines show contours of particle mass fraction, indicating that a region of low particle concentration exists just behind the wire and extends downstream. For smaller particles, the diffusion coefficient increases, causing a flux into this region of low concentration, and decreasing the downstream distance to which this depleted region extends.

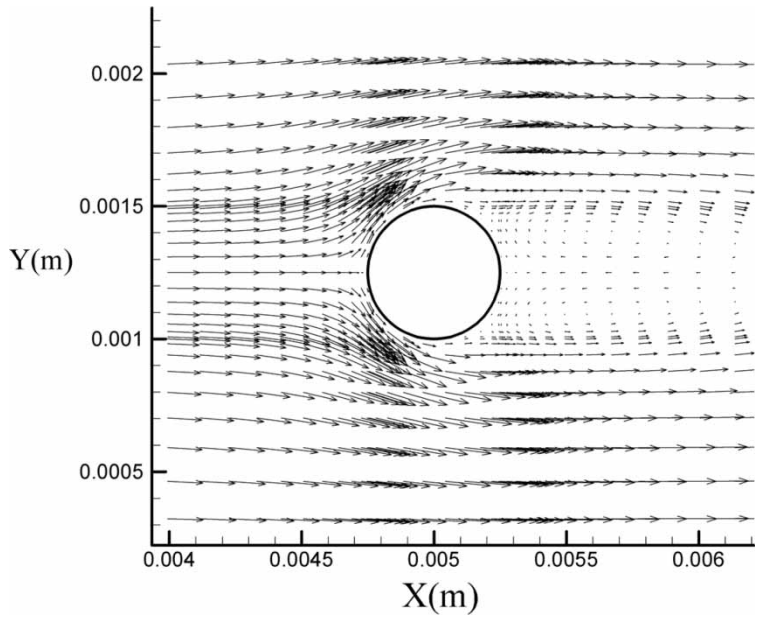

Figure 2. Flow field near the magnetic filter wire (thick, circular outline in the center). Vectors show fluid velocity.

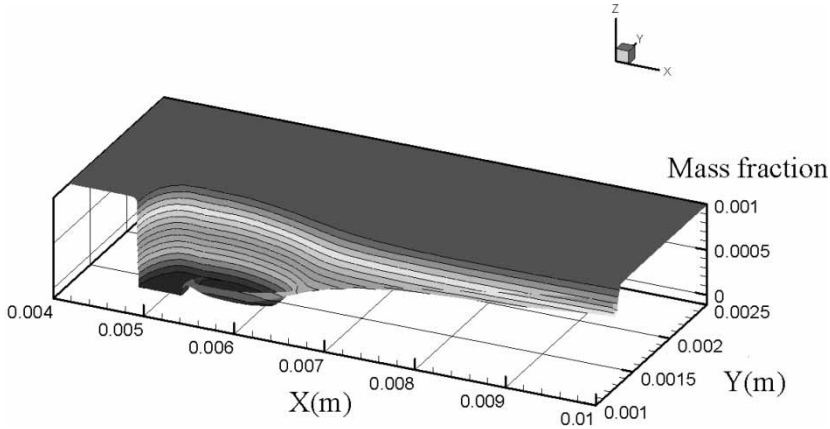

Figure 3. Three-dimensional contours of particle mass fraction.

Figure 4 shows the angular distribution of the particle mass flux density, $\rho\vec{u}\phi$, around the wire. This distribution indicates the amount of captured particle mass per unit time and unit area at each location on the wire surface. The flux is essential to estimate buildup on a wire surface (23, 28), which is an important problem for HGMS, because the buildup determines efficiency and breakthrough time of filters. The angular distribution of the particle mass flux density appears jagged, because COMPACT uses orthogonal coordinates to discretize (1), which produces a staircase representation of the control-volume faces.

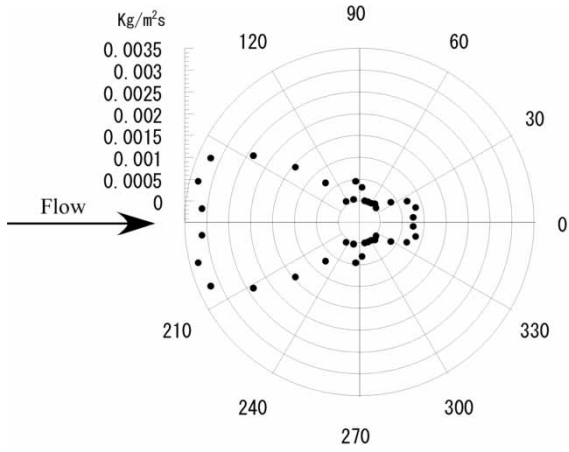

Figure 4. Angular distribution of particle capture ratio. The particle capture ratio represents the particle flux to a magnetic wire. The arrow shows the fluid flow direction.

Figure 4 shows locations where particles are captured. The wire mainly captures particles on the upstream side. Note, however, that a finite accumulation also occurs at the downstream side of the wire, because the recirculation zone brings particles from the free-stream close enough to the wire that they are captured. The strength of the recirculation zone increases with increasing axial fluid velocity, so that the particle flux downstream of the wire also increases with increasing axial fluid velocity. Because the other sides of the wire repulse paramagnetic particles as discussed previously, the mass flux is zero. Some positive values of mass flux appear in the repulsive regions. We expect that this is caused by error because of applying rectangular control-volumes to the circle.

Concentration Profiles and Capture ratio for Multiple Wires

In this section we compare our calculations for two wire arrangements: a rectangular lattice arrangement shown in Fig. 5 and a rhombic lattice arrangement shown in Fig. 6. In each arrangement, wires are located at lattice points. For all the following calculations, the wires had the same packing number density per unit area. The dotted lines in Figs. 5 and 6 indicate the calculation domain we used for the simulations. We used a periodic boundary condition on boundaries in the y-direction.

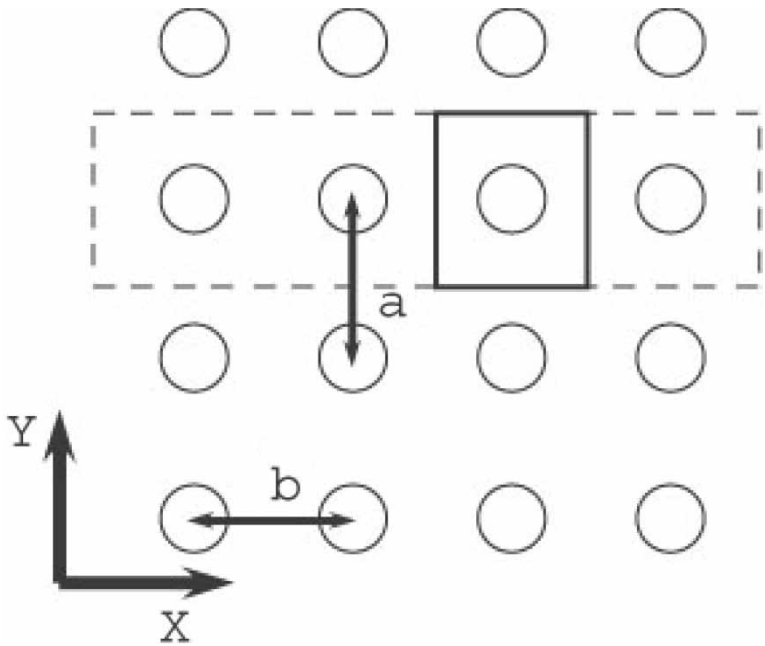

Figure 5. Schematic of a rectangular lattice arrangement of filter wires.

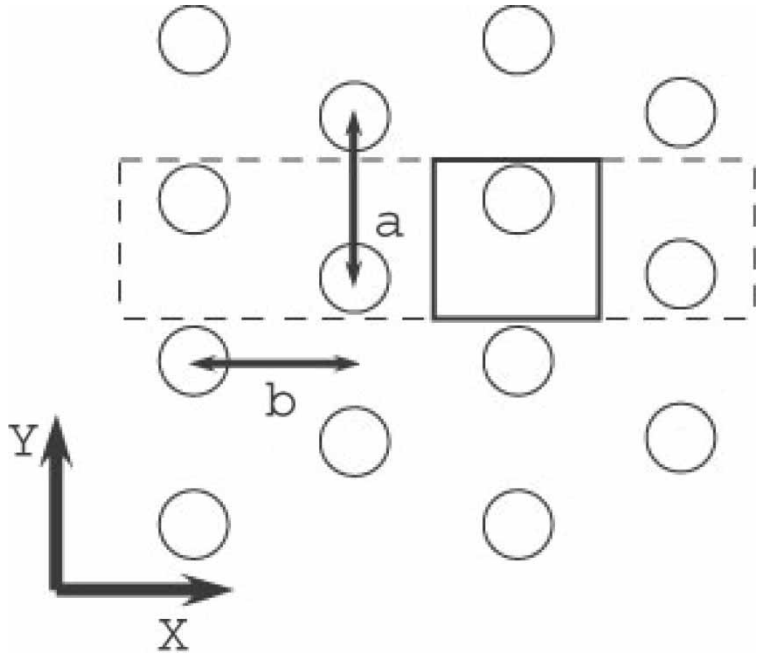

Figure 6. Schematic of a rhombic lattice arrangement of filter wires.

The solid-line squares in the calculation domains in Figs. 5 and 6 show examples of bounds around the wire to calculate the flux flowing to the wire. For simplicity we assumed that two sides of the bounds are on boundaries of the calculation domain and the other sides are parallel to the Y-axis. The flux density crossing the borders on boundaries of the calculation domain, however, is zero because of the periodic boundary conditions. To calculate the total flux to each wire, we calculate the flux only at the upstream and downstream bounds. When we calculate the capture ratio of a wire with (5), J_{in} is the total flux at the upstream bounds and J_{out} is the total flux at the downstream bounds.

To explicitly show effects of multiple wires, we show calculations of thinner filter wires packed densely, and the inlet velocity is larger than the previous simulation.

Circles show locations of wires, and “a” and “b” are distances between wires in the cross-stream and axial directions, respectively. The region enclosed by the dotted line represents the calculation domain. The square defined by the solid line is the bounds of the wire used to calculate the particle flux to the wires.

Circles show locations of wires, and “a” and “b” are distances between wires in the cross-stream and axial directions, respectively. The region enclosed by the dotted line represents the calculation domain. The square

defined by the solid line is the bounds of the wire used to calculate the particle flux to the wires.

Figures 7 and 8 show the particle mass fraction distribution for the cubic and rhombic lattice arrangements, where $a = 0.254\,\text{mm}$, $b = 0.79\,\text{mm}$, and the intensity of magnetic field, $|\mu_0 H| = 5\,\text{T}$. The diameter of the wires was $100\,\mu\text{m}$ and the inlet velocity was $0.265\,\text{m/s}$ ($\text{Re} = 25$). In these simulations the calculation domain contained 10 wires, but Figs. 7 and 8 show only a part of the complete calculation domain.

The single-wire simulations represent a filter composed of multiple wires side by side, whereas the rectangular and rhombic lattices represent the effect of multiple wires in the axial direction. The results for multiwire cases shown in Figs. 7 and 8 indicate that downstream wires capture a decreasing amount of particles, because these wires are in a fluid wake that is partially depleted of particles. In these calculations distributions of magnetic fields and flow velocity are calculated, including the effect of multiwires.

Figure 9 shows capture ratio of each wire. The capture ratios of the first wires in both the rectangular and rhombic lattices are nearly equal, because there are no upstream wires to affect them. The simulated capture ratio of these upstream wires is about 0.015. The capture ratio estimated by an analytical approximation of the Particle Trajectory model (45) is around 0.012. Because the conditions of the first wire are similar to them of a single wire in the Particle Trajectory model, the capture ratios of two models are consistent.

Because the upstream wires cause the particle mass fraction to decrease and to distribute unevenly, the particle mass fraction available for the downstream wires decrease, and the capture ratio of the downstream wires is therefore lower than for the upstream wires. These results show that our model takes account of multiwires effect precisely.

In the rhombic lattice arrangement, the distance between wires in the axial direction is longer than in the rectangular lattice configuration, and

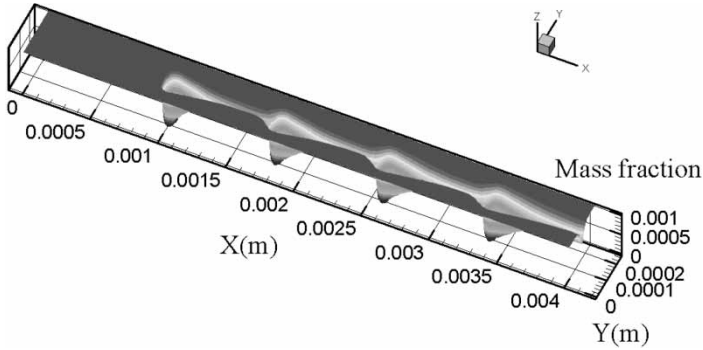

Figure 7. Distribution of particle mass fraction for a rectangular lattice arrangement. Particle mass fraction near the upper four wires is shown.

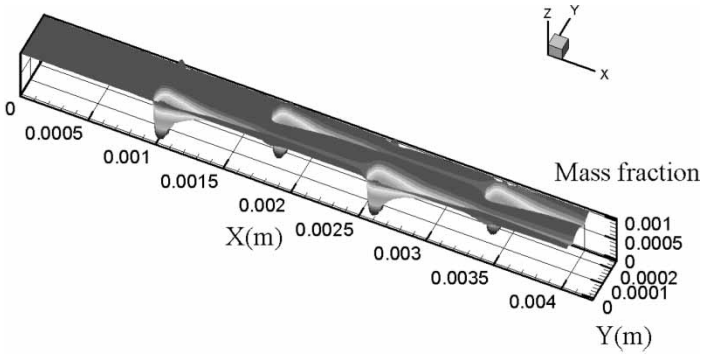

Figure 8. Particle mass fraction for a rhombic lattice arrangement. Particle mass fraction near the upper four wires is shown.

therefore in the rhombic lattice arrangement there is more time for particles to diffuse into the depleted particle region before the next wire is encountered. This increases the capture ratio of each wire and maintains a consistently higher capture ratio downstream for the rhombic lattice arrangement, compared with the rectangular lattice arrangement.

For either wire arrangement, we expect that the capture ratio decreases monotonically toward a limiting capture ratio, but that the limiting capture

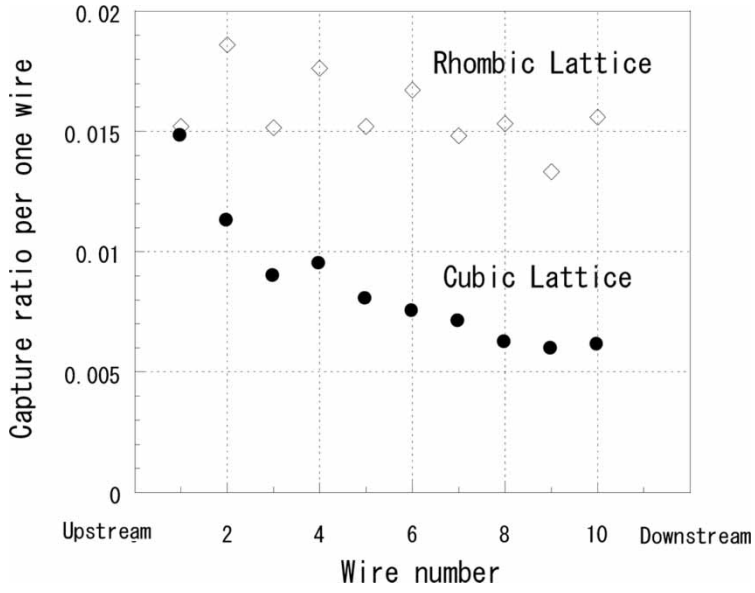

Figure 9. Capture ratio per wire as a function of axial position, for rectangular and rhombic lattice arrangements.

ratio for the rhombic lattice wire arrangement will be higher than for the rectangular lattice arrangement. These limiting values should correspond to the average capture ratio per wire measured for actual magnetic filters.

Effect of Magnetic Field Intensity

Figure 10 shows the capture ratio per wire for $|\mu_0\vec{H}| = 2$ and 5 T and indicates that a stronger magnetic field increases the capture ratio. Because the wires are made of stainless steel, they are saturated below 2 T. For paramagnetic particles, magnetization increases in proportion to magnetic field strength. In this simulation, capture ratios increased because of an increment in the magnetization of particles.

Compared with the capture ratio at a field strength of 2 T, at a field strength of 5 T the capture ratio decreases faster with increasing wire axial position, because the particle capture rate increases with increasing field strength.

Because the results shown in Fig. 10 indicate that for a given total capture ratio, particle capture ratio per wire is lower for $|\mu_0\vec{H}| = 2\,\mathrm{T}$ than for $|\mu_0 H| = 5\,\mathrm{T}$, for lower magnetic fields, a longer wire matrix is required than for $|\mu_0 H| = 5\,\mathrm{T}$. This implies that the separation system must provide additional energy to pump the water through a longer channel, which creates

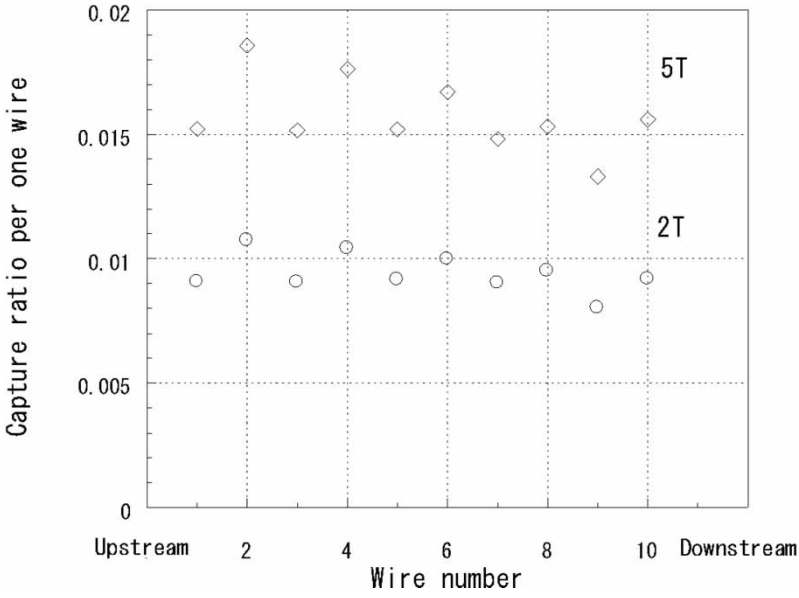

Figure 10. Capture ratio per wire for $|\mu_0\vec{H}| = 2$ and 5 T for rhombic lattice configuration.

a larger pressure drop. In addition, use of higher magnetic fields also permits smaller separation devices to be used.

Effect of Fluid Velocity

Figure 11 shows the dependence of capture ratio on fluid velocity. The capture ratio is shown for fluid velocities of 0.067, 0.133, and 0.267 m/s and a magnetic field strength of 5 T. As the fluid velocity decreases, the capture ratio increases and decreases faster in the axial direction than for higher fluid velocities. This is because for lower fluid velocities each wire captures an increasing number of particles.

Effect of Combination of Magnetic Field and Flow Velocity

In this section we show that an increment of magnetic field and a decrement of fluid velocity yield the same effect in magnetic filters.

Figure 12 shows combinations of magnetic field and fluid velocity when wires in a rhombic lattice have nearly equal capture ratio. The capture ratio of each wire at the same location is equal. Namely, this limited calculation suggests that an increment of magnetic field intensity affects a capture ratio of each wire the same as a decrement of fluid velocity. This relation is suggested by the Particle Trajectory model, because the magnetic velocity defined in the Particle Trajectory model (13–21) appears as the dimensionless

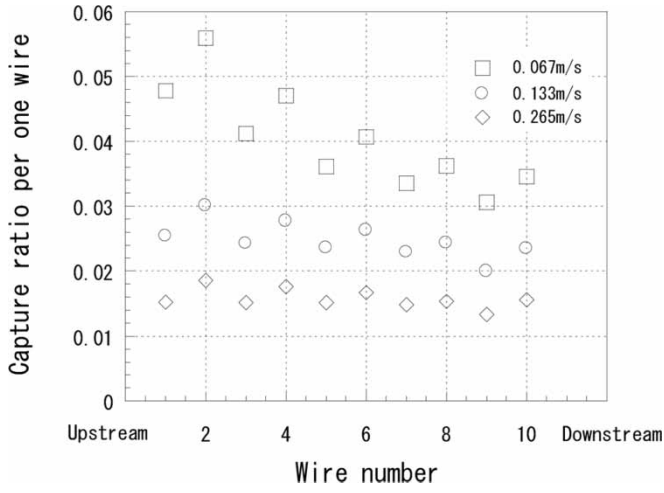

Figure 11. Capture ratio per wire at 5 T as a function of fluid velocity and axial location in the rhombic lattice configuration.

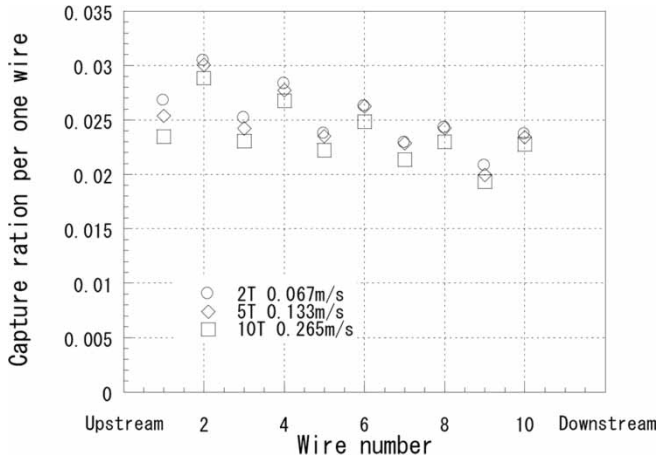

Figure 12. Capture ratio per wire at magnetic field/fluid velocity pairs of 2 T/0.067 m/s, 5 T/0.133 m/s, and 10 T/0.267 m/s.

variable, v_m/v_f, in an analytic approximation form of the capture radius, where v_m is the magnetic velocity and v_f is flow velocity of fluid. Because v_m is proportional to the magnetic field intensity, capture radius or capture ratio is a function of $|\mu_0 H|/v_f$.

CONCLUSIONS AND FUTURE RESEARCH

The calculation results demonstrated that our model can simulate HGMS precisely. The coincidence of capture ratios for a single wire and function of capture ratio on magnetic field intensity and flow velocity suggests that our model include the Particle Trajectory model.

The outward form of the data in Fig. 4 indicates the shape of the particle deposits, which is similar to the shape of observed particle deposits. To accurately simulate the shape of deposits, however, the time-dependent particle accumulation rate must also be simulated, because particle deposits affect the flow pattern and magnetic fields in the vicinity of the wires, and therefore affect the particle capture ratio and angular distribution around the wires. We are continuing with these types of simulations.

For a given design efficiency, many combinations of magnetic field strength and fluid velocity can be used in an HGMS system. For a given volume of treatment fluid, however, a higher-intensity magnetic field permits shorter filtering times and more compact systems. We expect that our model help to design suitable HGMS devices.

Because particles deposit preferentially on the upstream wires as shown in Section III, the wire matrix preferentially becomes saturated with particles

in the upstream part and increases the pressure drop before all of the wires are saturated with particles. Figure 12 suggests that the capture ratio or deposition on each wire can be controlled by specifying a combination of the magnetic field and fluid velocity for a given capture ratio of the magnetic filter.

The knowledge gained by these types of simulations can be used to improve HGMS systems, because typical experiments cannot reveal the detailed dynamics occurring in the vicinity of individual wires. Our proposed model, however, reveals distributions of fluid flow, magnetic fields, and particle concentrations near magnetic filter wires. Our model can also account for the effect of neighboring wires.

REFERENCES

1. Kolm, H.H. US patent 3,567,026, 1971 and 3,676,337, 1972.
2. Oberteuffer, J.A. (1973) High gradient magnetic separation. *IEEE Trans. Magn.*, MAG-9, 303–306.
3. Kelland, D.R. (1973) High gradient magnetic separation applied to mineral beneficiation. *IEEE Trans. Magn.*, MAG-9, 307–310.
4. Iannicelli, J. (1982) Development of high extraction magnetic filtration by the kaolin industry of Georgia. *IEEE Trans. Magn.*, MAG-12, 489.
5. Yano, J. and Eguchi, I. (1978) Application of high gradient magnetic separation for water treatment in steel industry. In *Industrial Application of Magnetic Separation*; Liu, Y.A., ed.; IEEE Inc., 134–136, 78CH1447–2 MAG.
6. Heitmann, H.G.. Studies of the application of electromagnetic filters in power plants. *ibid.*188–196.
7. Okada, H., Fukushima, K., and Tamura, J. (1999) Magnetic separation of fine colloidal magnetite particles by a superconducting magnet. *Trans. IEE of Japan*, 119-B: 1181–1186, in Japanese.
8. Kitazawa, K. (2001) Current trends of superconductivity technology. *Oyo Buturi*, 70: 3–13, Japanese.
9. Hultgren, A., Chen, C.S., Meyer, G.J., and Reich, D.H. (2004) Cell manipuration using magnetic nanowires J. *Appl. Phys.*, 93: 7554–7556.
10. Thurm, S. and Oldenbach, S. (2002) Magnetic separation of ferrofluids J. *Magn. Magn. Mater.*, 252: 247–249.
11. Wang, H., Liu, Q., Zhang, J., and Hsu, T.Y. (2003) The size effecton the phase stability of nanograied Fe-12Ni powders and the magnetic separation of face-centered-cubic-body centered-cubic phases *Namotechnology*, 14: 696–700.
12. Ritter, J.A., Ebner, A.D., Daniel, K.D., and Stewart, K.L. (2004) Application of high gradient magnetic seapration principles to magnetic drug targeting. *J. Magn. Magn. Mater.*, 280: 184–201.
13. Watson, J.H.P. (1973) Magnetic filtration. *J. Appl. Phys.*, 44: 4209–4213.
14. Watson, J.H.P. (1975) Theory of capture of particles in magnetic high-intensity filters. *IEEE Trans. Magn.*, MAG-11: 1597–1599.
15. Luborsky, F.E. and Drummond, B.J. (1975) High gradient magnetic separation: Theory versus experiment. *IEEE Trans. Magn.*, MAG-11: 1696–1700.
16. Birss, R.R., Gerber, R., and Parker, M.R. (1976) Theory and design of axially ordered filters for high intensity magnetic separation. *IEEE Trans. Magn.*, MAG-12: 892–894.

17. Uchiyama, S., Kondo, S., Takayasu, M., and Eguchi, I. (1976) Performance of parallel stream type filter for HGMS. *IEEE Trans. Magn.*, MAG-12: 895–897.
18. Lawson, W.F., Simons, W.H., and Treat, R.P. (1977) The dynamics of a particle attracted by a magnetized wire. *J. Appl. Phys.*, 48: 3213–3224.
19. Hayashi, K. and Uchiyama, S. (1980) On particle trajectory and capture efficiency around many wires. *IEEE Trans. Magn.*, MAG-16: 827–829.
20. Simons, W.H. and Treat, R.P. (1980) Particle trajectories in a lattice of parallel magnetized fibers. *J. Appl. Phys.*, 51: 578–588.
21. Ohara, T. (1984) Particle capture theory and experiment on an amorphous magnetic ribbon filter. *IEEE Trans. Magn.*, MAG-20: 436–443.
22. Natenapit, M. (1995) Effective medium treatment of laminar flow in magnetic filteration. *J. Appl. Phys.*, 78: 4353–4359.
23. Badescu, V., Murariu, V., Rotariu, N., and Rezlescu, N. (1996) A new modeling of the initinal buildup evolution on a wire in an axial HGMF filter. *J. Magn. Magn. Mater.*, 163: 225–231.
24. Badescu, V., Rotariu, O., Murariu, V., and Rezlescu, N. (1997) Transverse high gradient magnetic filter cell with bounded flow field. *IEEE Trans. Magn.*, Mag-33: 4439–4444.
25. Natenapit, M. and Sanglek, W. (1998) Capture radius of magneitc particles in random cylindrical matrices in high gradient magnetic separation. *J. Appl. Phys.*, 85: 660–664.
26. Markus, F. and Franzereb, M. (1998) Determination of the capture radii of magnetite bearig hydroide flocs in magneitc filtaration. *IEEE Trans. Mag.*, Mag-34: 3902–3909.
27. Murariu, N., Rezlescu, V., Rotariu, N., and Badescu, V. (1998) Concentration influence on recovery in a high gradient magneitc separation axial filter. *IEEE Trans. Mag.*, Mag-34: 695–699.
28. Murariu, N., Rezlescu, V., Rotariu, N., and Badescu, V. (1998) The effect of suspension concentration on the buildup evolution in a HGMF-axial magneit filter. *Eur. Phys. J. Ap.*, 1: 39–44.
29. Abbasov, T., Herdem, S., and Koeksal, M. (1999) Praticle capture in axial magneitc filters with power law flow model. *J. Phys. D.*, 32: 1097–1103.
30. Herdem, S., Abbasov, T., and Koeksal, M. (1999) Modelling of the buildup process of particles in pores of high gradient magneitc filters using the Fokker-Planck equation. *J. Phys. D.*, 32: 3146–3150.
31. Vincent-Viry, O., Mailfert, A., Gillet, G., and Diot, F. (2000) Magnetic percolation phenomenon in high-field high-gradient separators. *IEEE Trans. Mag.*, Mag-36: 3947–3952.
32. Sido, N.M., Mailfert, A., Gillet, G., and Colteu, A. (2003) Study of high intensity magneitc separation process in grooved palte matrix. *Eur. Phys. J. Appl.*, 24: 201–207.
33. Takayasu, M., Gerber, R., and Friedlaender, F.J. (1983) Magnetic separation of submicron particles. *IEEE Trans. Magn.*, MAG-19: 2112–2114.
34. Gerber, R., Takayasu, M., and Friedlaender, J.F. (1983) Genaralization of HGMS theory: The capture of ultra-fine praticles. *IEEE Trans. Magn.*, MAG-19: 2115–2117.
35. Gerber, R. (1984) Magnetic separation of ultra-fine particles. *IEEE Trans. Magn.*, MAG-20: 1159–1164.
36. Kramer, A.J., Janssen, J.J.M., and Prenboom, J.A.A.J. (1990) Single-wire HGMS of colloidal particles: The evolution of concentration profiles. *IEEE Trans. Magn.*, MAG-26: 1858–1860.

37. Davies, L.P. and Gerber, R. (1990) 2-D simulation of ultra-fine particle capture by a single-wire magnetic collector. *IEEE Trans. Magn.*, MAG-26: 1867–1869.
38. Patankar, S.V. (1980) *Numerical Heat Transfer and Fluid Flow*; Taylor and Francis.
39. Patankar, S.V. (1980) A calculation procedure for two-dimensional elliptic situations. *Numerical Heat Transfer,*, 4: 409.
40. Watson, J.H. and Bahaj, P.A.S. (1989) Vortex capture in high gradient magnetic separators at moderate reynolds number. *IEEE Trans. Magn.*, Mag-25: 3803–3805.
41. Li, Z. and Watson, J.H.P. (1996) Technical notes an experimental study with a vortex magnetic separation (VMS) device. *Minerals Engineering*, 9: 367–371.
42. Watson, J. and Li, H.P.Z. (1997) Vortex magnetic separation. *Proc. Inst. Mech. Enginrs.*, 211, Part E: 31–42.
43. Karki, K.C., Whitby, E.R., Patankar, S.V., Winstead, C., Ohara, T., and Wang, X. (2001) A numerical model for magneitc chormatgraphy. *Appl. Math. Model.*, 25: 355–373.
44. Mitsuhashi, K., Yoshizaki, R., Ohara, T., Matsumoto, F., Nagai, H., and Wada, H. (2002) Retension of ions in a magnetic chromatograph using high-intensity and high-gradient magnetic fields. *Sep. Sci. Tech.*, 37: 3635–3645.
45. Uchiyama, S. and Hayashi, K. (1978) *Industrial Application of Magnetic Separation*; Liu, Y.A., ed.; IEEE Inc.: New York, 169.